Scientific
Research
Publishing

Structural and Elastic Behavior of Chromium Doped $Pr_{0.5}Sr_{0.5}MnO_3$ System

Ashok Kumar Kusuma[1,2], Elle Sagar[1,3], G. Sreeram Reddy[3], K. Vijaya Kumar[1*]

[1]Department of Physics, JNTU Hyderabad, Hyderabad, India
[2]B V Raju Institute of Technology, Narsapur, India
[3]Vidya Jyothi Institute of Technology, Hyderabad, India
Email: *kvkphd@gmail.com

Abstract

A series of colossal magneto resistance (CMR) materials with compositional formula $Pr_{0.5}Sr_{0.5}Mn_{1-x}Cr_xO_3$ (x = 0, 0.1, 0.2, 0.3, 0.4) were prepared by sol-gel technique using pure metal nitrates as the starting materials. These samples were characterized structurally by X-ray diffraction, FTIR and SEM. All the samples exhibit orthorhombic structure without any detectable impurities. The bulk densities for all the compositions were measured from the pellets. The Young's and Rigidity moduli, Poisson's ratio and Debye temperature of all the compositions were calculated with the experimentally measured ultrasonic longitudinal and shear velocities at room temperature using pulse transmission technique. As the materials are porous, zero porous elastic moduli have also been calculated using a well-known Hasselmann and Fulrath model. The observed variation of elastic moduli with varying chromium doping concentration has been studied qualitatively.

Keywords

CMR Materials, Resistivity, Ultrasonic Velocity, Elastic Moduli

1. Introduction

Colossal Magneto Resistance (CMR) manganites are capable of exhibiting the coexistence of metallic conductivity along with ferromagnetic behavior at low temperatures (below T_C) and insulating behavior along with paramagnetic behavior at high temperatures (above T_C). The double exchange mechanism was used by Zener [1] to explain correlation between metallic conductivity and ferromagnetism in these materials. Further Millis *et al.* [2], suggested that the double exchange mechanism alone cannot account for the magnitude of the resistivity drop

below *T*c and the electron-phonon coupling, originally due to Jahn Teller distortion, might also play an important role among CMR materials. Thus, this most interesting motivating and effective behavior exhibited by CMR materials fascinated research community in studying structural, magnetic and electrical transport properties and their potential applications in memory devices [3] [4] [5]. Among these CMR materials, the charge-ordered phase in half-doped manganites, with compositions, $R_{0.5}A_{0.5}MnO_3$ (R = La, Pr, Sm, and Nd; A = Sr and Ca) exhibit interesting phenomena such as charge, orbital, and spin ordering, along with magnetic and electric field driven transitions [6] [7]. Moreover, it was reported that doping with Cr in the place of Mn site is an effective way to modify the charge ordered (CO)/orbital ordered (OO) and anti-ferromagnetic insulating (AFMI) phases. As the Cr^{3+} ion is iso-electronic with Mn^{4+} ion, Mn site substitutions with Cr in manganites have attracted great interest. Magnetic impurities such as Cr and Ru at the Mn site can effectively induce both metallicity and ferromagnetism in the insulating antiferromagnetic $R_{0.5}A_{0.5}MnO_3$ (A = Ca, Sr) [8] [9]. It was reported that among the dopants, chromium is the most efficient one to induce a metal insulator transition in charge ordered undoped insulators, and lead to a much higher CMR effect [10] [11] [12].

Finally, in the theory of solids, study of the elastic behavior has particular significance in understanding the nature of inter atomic and inter ionic forces in them [13]. Further, the general idea of elastic moduli values that characterize mechanical strength, fracture toughness and thermal shock resistance will be useful in study the high strains that might develop when ceramic perovskites are subjected to a high magnetic field [14]. Moreover, the ultrasonic velocity measuring technique is a non-destructive one and is a very sensitive tool not only for studying the defects of microscopic process in solids but also most conventional technique for determination of elastic constants [15]. In view of this, the influence of Cr ion doping on structural and elastic behavior of $Pr_{0.5}Sr_{0.5}Mn_{1-x}Cr_xO_3$ (x = 0, 0.1, 0.2, 0.3 & 0.4) system is presented in this article.

2. Experimental Details

Polycrystalline $Pr_{0.5}Sr_{0.5}Mn_{1-x}Cr_xO_3$ (x = 0, 0.1, 0.2, 0.3 & 0.4) samples were synthesized by the sol-gel method [16] using pure metal nitrates as the initial materials (99.9% pure). The compositions of the samples are henceforth designated as PSMCO-0, PSMCO-1, PSMCO-2, PSMCO-3 and PSMCO-4 respectively. These powders were calcinated at 1100°C for 8 h followed by sintering at 1300°C for 4 h in air. The structural characterization was carried out by powder X-ray diffraction (XRD) using Phillips expert diffractometer at room temperature in the 2θ range of 20° - 80°. The bulk densities of all the samples were calculated by means of immersion method. With the help of these bulk densities and X-ray densities, the porosity values were measured. Micro structural studies of the samples were carried out using a Scanning Electron Microscope. Fourier transform infrared spectroscopy (FTIR) was recorded on a Jasco FTIR spectrometer (Model: FT/IR-4200typeA) within a range of 400 - 4000 cm^{-1}.

The longitudinal and shear wave velocity values were calculated by ultrasonic pulse transmission technique using a pulse generator RPR-4000 (RITEC INC., USA). The pulse oscillator generates RF pulses and a transmitting transducer converts them into acoustic pulses. The acoustic pulses propagating through the disc shaped testing sample of thickness ~2.5 mm and diameter ~10 mm, these pulses will convert into electrical signals at the receiving transducer. The amplified output signals are displayed on a storage oscilloscope. Quartz transducers with ability to generate ultrasonic signals of 1 MHz were used for the both the operations like generating and detecting signal. The longitudinal and shear wave signals can be generated by using X and Y-cut transducers respectively. The transmission time of the ultra sound was measured up to an accuracy of 1 μs using a 100 MHz digital storage oscilloscope (Tektronix model: TDS2012C). The overall correctness of these measurements in velocity is about 0.25% and elastic moduli are about 0.5%. The block diagram of ultrasonic pulse transmission technique is shown in **Figure 1**.

3. Results and Discussions

3.1. Structural Characterization

3.1.1. X-Ray Diffraction

X ray diffraction patterns of all the samples are shown in **Figure 2(a)**. A systematic investigation of the XRD data clearly reveals that all the samples are having single phase without any noticeable impurity. Rietveld refinement technique [17] was used to analyze the XRD data by assuming orthorhombic structure (*Pnma* space group). The Rietveld refinement is fitted for the graph of PSMCO-0 sample and is shown in **Figure 2(b)**. The tailored parameters of all the samples are given in **Table 1**. As per the earlier reports [18], in the case of lattice parameters, a systematic variation with Cr doping is not noticed and the same behavior is observed in the present study also. This may be attributed to the fact that there is a minor difference between the ionic radii of Cr^{3+} and Mn^{3+} [19].

(1) Pulse generator, (2) Acoustic transducer, (3) Sample, (4) Preamplifer,

(5) C.R.O (6) Syncronising generator

Block diagram of Pulse transmission technique
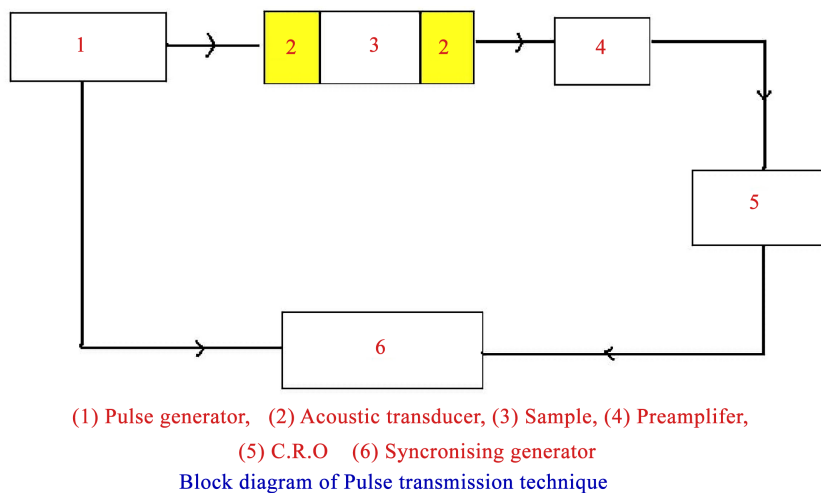
Figure 1. Block diagram of pulse transmission technique.
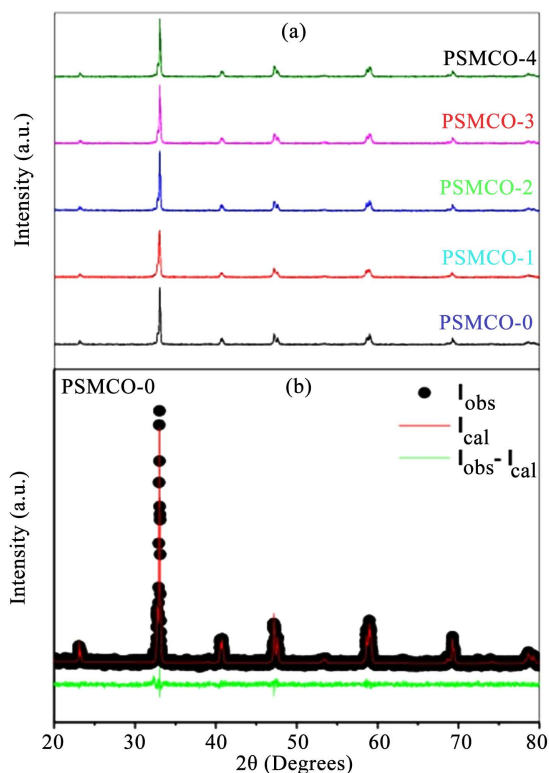
Figure 2. (a) XRD patters of Cr doped $Pr_{0.5}Sr_{0.5}$ MnO_3 system; (b) Reitveld refined XRD pattern of PSMCO-0 sample. Circles indicate; (c) Experimental points while Red line indicates refined data and the green line indicates difference between experimental and refined data.

Table 1. Crystallographic data of Cr doped $Pr_{0.5}Sr_{0.5}MnO_3$ system.

Sample code→ Parameters ↓	(PSMCO-0)	(PSMCO-1)	(PSMCO-2)	(PSMCO-3)	(PSMCO-4)
a (Å)	5.4218	5.4228	5.4275	5.4205	5.4268
b (Å)	7.6312	7.6325	7.6384	7.6302	7.6388
c (Å)	5.4618	5.4605	5.4595	5.4648	5.4632
R_P (%)	7.21	7.18	7.34	6.74	7.24
R_{WP} (%)	9.19	8.95	9.47	9.61	9.44
R_{EXP} (%)	8.89	8.80	9.07	9.40	9.45
Goodness of fit (S)	1.03	1.01	1.04	1.02	1.03

3.1.2. Scanning Electron Microscopy

The micro structural investigation of all the samples was carried out using a Scanning Electron Microscope and the micrographs of the samples are shown in **Figure 3**. It is interesting to note that the grain sizes of parent compound PSMCO-0 are small and are in the range of 50 - 80 nm. It can also be seen from the micrographs that the shape of the grains of all the samples are not having any particular pattern. It is interesting to note that with increasing Chromium content, the grain size is also increased.
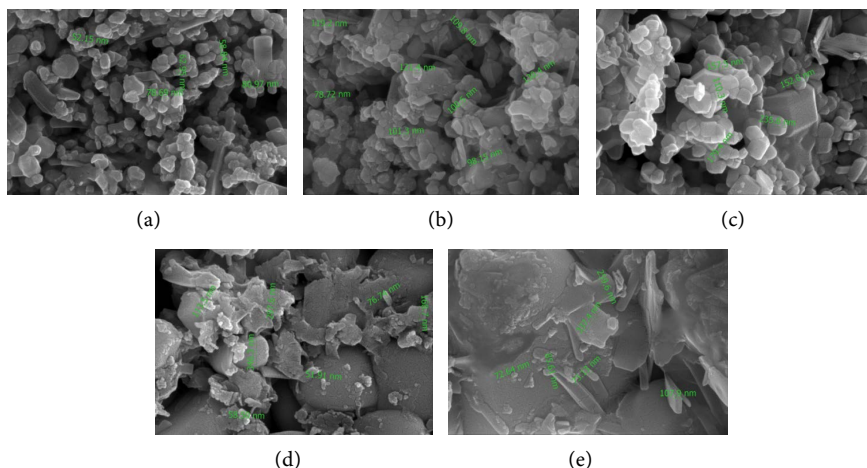
Figure 3. SEM images of Cr doped $Pr_{0.5}Sr_{0.5}MnO_3$ system. (a) PSMCO-0; (b) PSMCO-1; (c) PSMCO-2; (d) PSMCO-3 and (e) PSMCO-4.

3.1.3. FTIR Spectra

The FTIR transmission spectra of Cr doped PSMO samples are presented in Figure 4, which represents the chemistry for the formation perovskite materials. The absorption peak at 600 cm^{-1} corresponds to stretching of the metal-oxygen bond in the perovskite, which involves the internal motion of a change in Mn-O-Mn bond length in MnO_6 octahedral. Interestingly the position of this absorption band is shifted towards higher frequency side up to PSMCO-3 then decreased. The broad absorption peak at 3350 cm^{-1} is the characteristic of absorbed water or hydroxyl group in the alcohol. A band at 1100 cm^{-1} reveals the formation of CH_3-CH_3-, CH_3-NH_2-, CH_3O-bands when the polymerization takes place with metal nitrate, citric acid, and ethylene glycol. The peak at 1115.39 cm^{-1} is attributed to the C-C-O structure from ethylene glycol in the polymerization process.

3.2. Ultrasonic Velocity Studies

The longitudinal and shear wave velocities (V_l & V_s) values of all the samples are presented in Table 2, and are found to increase continuously with doping concentration of Cr and the behavior is in consistence with earlier reports of some other CMR materials [20] and manganites [13]. With the support of velocity values, Poisson's ratios (σ) of all the samples were calculated by the well-known relation [14], and the calculated values are given in Table 2.

$$\sigma = \frac{V_l^2 - 2V_s^2}{2\left(V_l^2 - V_s^2\right)} \tag{1}$$

Further the Poisson's ratio values are found to be in the range, 0.24 - 0.28 for different compositions. The elastic moduli values were also measured using the well-known methods [14] and the values are given in Table 3. The Young's modulus and rigid moduli values of all the samples are found to increase with the increasing doping concentration of dopant ion and the same behavior was detected earlier in some other CMR materials [20] [21].
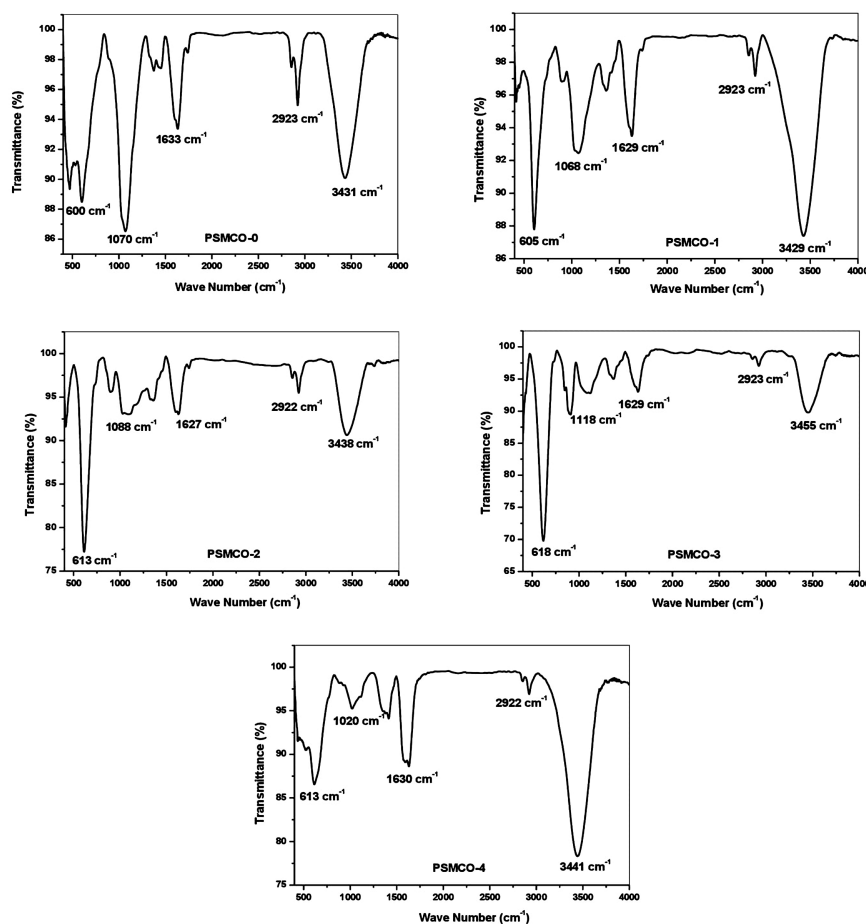
Figure 4. FTIR vibration spectrum of Cr doped $Pr_{0.5}Sr_{0.5}$ MnO_3 system.

Table 2. Porosity percentage and ultrasonic velocities of Cr doped $Pr_{0.5}Sr_{0.5}$ MnO_3 system.

Parameters→ Sample code ↓	Bulk density (ρ_b)	X-ray density (ρ_x)	Porosity %	V_l (m/sec)	V_s (m/sec)	σ	θ_D
(PSMCO-0)	4462	6383	30.0	2984	1642	0.28	331.7
(PSMCO-1)	4955	6373	22.0	3425	1986	0.24	357.1
(PSMCO-2)	5071	6356	20.2	4273	2392	0.27	421.0
(PSMCO-3)	5457	6338	13.9	4666	2566	0.28	422.4
(PSMCO-4)	5546	6352	12.6	5000	2800	0.27	454.9

Table 3. Elastic constants of Cr doped $Pr_{0.5}Sr_{0.5}$ MnO_3 system before and after porosity corrections.

Parameters→ Sample code ↓	Before Porosity correction		After Porosity correction	
	E (GPa)	G (GPa)	E_0 (GPa)	G_0 (GPa)
(PSMCO-0)	30.79	12.03	77.3	28.54
(PSMCO-1)	48.45	19.54	86.68	34.42
(PSMCO-2)	73.68	29.01	123.86	47.67
(PSMCO-3)	91.98	35.93	127.53	49.08
(PSMCO-4)	110.43	43.46	147.77	57.5

3.3. Porosity Correction

The elastic properties of any material depend on the density and the porosity percentage of the testing samples [14]. As the samples of the present investigation are prepared by the well-known sol-gel method, they exhibit ceramic nature with porosity. It is important to measure the percentage of porosity in these materials. The porosity values were calculated from bulk density and XRD densities of the samples and the measured porosity values are presented in Table 2. The porosity percentage of all the samples is found to have in the range of 12% - 30%. As all the samples under the study are found to be porous, the measured elastic moduli will be less than those of non-porous ones and as such of these values do not have any significance unless they are corrected to zero porosity [14] [20]. For this to resolve, Hasselman and Fulrath model has been used [22]. This model proposed on the assumption that the samples prepared by solid state reaction method can mainly posses spherical type of pores. According to this model [22], Young's and shear wave moduli can be specified by,

$$E_0 = \frac{E}{1-\alpha_E P}; \text{ where } \alpha_E = \frac{3(9+5\sigma)(1-\sigma)}{2(7-5\sigma)} \tag{2}$$

$$G_0 = \frac{G}{1-\alpha_G P}; \text{ where } \alpha_G = \frac{15(1-\sigma)}{7-5\sigma} \tag{3}$$

where E_0 and G_0 are the Young's and Rigidity moduli of non-porous matrix respectively, whereas E and G are the experimental measured values of Young's and rigidity moduli respectively, and P is porosity of the material. By means of Equations (2) and (3), porosity corrections have been completed for the experimental elastic moduli and are the zero porous values are presented in Table 3. From Table 3, one may see that the values of Young's modulus values are found to increase continuously with doping concentration which conforms with the similar behavior reported earlier in the case of some manganite based materials [20] [21].

3.4. Acoustic Debye Temperature (θ_D) Values

Acoustic Debye temperature (θ_D) which can be calculated from mean sound velocities affords useful information about the physical properties of solids. The Debye temperatures of all the samples of the current investigation have been measured using Anderson's relation [22]

Debye temperature:

$$\theta_D = \frac{h}{k}\left[\frac{3N_A}{4\pi V_A}\right]^{1/3} \cdot V_m \tag{4}$$

where, h and k are Planck's and Boltzmann's constants respectively, N_A is the Avogadro's number, V_A is the mean atomic volume given by $(M/\rho)/q$ and M is the molecular weight, q is the number of atoms in the formula unit and V_m is the average sound velocity calculated using the formula [22]

Mean sound velocity:

$$V_m = \left[\frac{3\left(V_l^3 \cdot V_s^3\right)}{\left(V_s^3 + 2V_l^3\right)} \right]^{1/3} \tag{5}$$

The calculated values of Acoustic Debye temperature (θ_D) are given in Table 3 and are found to increase with increasing doping concentration.

3.5. Elastic Behavior in Terms of Strength

Usually, the elastic behavior of any oxide materials can be explained in terms of binding forces between various ions [13]. Depending upon the effect of dopant ion on the binding forces, the elastic moduli of a material system can increase or decrease continuously with increasing dopant concentration [23]. As the elastic moduli along with Debye temperatures of all the samples are found to increase continuously with increasing Cr concentration, the binding forces between various ions of these materials might be increasing continuously.

4. Conclusions

1) CMR materials with compositional formula $Pr_{0.5}Sr_{0.5}Mn_{1-x}Cr_xO_3$ (x = 0, 0.1, 0.2, 0.3 & 0.4) were synthesized without any detectable impurity and there is no systematic variation in the lattice parameters with the Cr doping is observed.

2) The grain size of parent compound is found to vary between 50 - 80 nm and for the remaining samples; the grain size is increased with doping concentration up to doping percentage of 30%.

3) Ultrasonic longitudinal and shear velocities were found to increase with increasing Cr concentration.

4) The zero porous elastic moduli were found to increase continuously with increasing Cr concentration.

5) It is clearly observed that the mechanical strength of the samples was found to be increased with the Cr concentration.

Acknowledgements

Conflicts of Interest

The authors declare no conflicts of interest regarding the publication of this paper.

References

[1] Zener, C. (1951) Interaction between the d-Shells in the Transition Metals. II. Ferromagnetic Compounds of Manganese with Perovskite Structure. *Physical Review Journals Archive*, **82**, 403-405. https://doi.org/10.1103/PhysRev.82.403

[2] Millis, A.J., Shraiman, B.I. and Mueller, R. (1996) Dynamic Jahn-Teller Effect and Colossal Magnetoresistance in $La_{1-x}Sr_xMnO_3$. *Physical Review Letters*, **77**, 175-178. https://doi.org/10.1103/PhysRevLett.77.175

[3] Dagotto, E., Hotta, T. and Moreo, A. (2001) Colossal Magnetoresistant Materials: The Key Role of Phase Separation. *Physics Reports*, **344**, 1-153. https://doi.org/10.1016/S0370-1573(00)00121-6

[4] Tokura, Y. (2006) Critical Features of Colossal Magnetoresistive Manganites. *Reports on Progress in Physics*, **69**, 797-851. https://doi.org/10.1088/0034-4885/69/3/R06

[5] Hatano, T. (2013) Gate Control of Electronic Phases in a Quarter-Filled Manganite. *Scientific Reports*, **3**, Article No. 2904. https://doi.org/10.1038/srep02904

[6] Jin, S., Tiefel, H., Mc Cornack, M., Fastnacht, R.A., Ramesh, R. and Chen, L.H. (1994) Thousand Fold Change in Resistivity in Magnetoresistive La-Ca-Mn-O Films. *Science*, **264**, 413-415. https://doi.org/10.1126/science.264.5157.413

[7] Autret, C., Maignan, A., Martin, C., Hervieu, M., Hardy, V., Hebert, S. and Raveau, B. (2003) Magnetization Steps in a Noncharge-Ordered Manganite, $Pr_{0.5}Ba_{0.5}MnO_3$. *Applied Physics Letters*, **82**, 4746-4748. https://doi.org/10.1063/1.1588756

[8] Raveau, B., Maignan, A. and Martin, C. (1997) Insulator-Metal Transition Induced by Cr and Co Doping in $Pr_{0.5}Ca_{0.5}MnO_3$. *Journal of Solid State Chemistry*, **130**, 162-166. https://doi.org/10.1006/jssc.1997.7373

[9] Kimura, T., Tomioka, Y., Okimoto, Y. and Tokura, Y. (1999) Diffuse Phase Transition and Phase Separation in Cr-Doped $Nd_{1/2}Ca_{1/2}MnO_3$: A Relaxor Ferromagnet. *Physical Review Letters*, **83**, 3940-3943. https://doi.org/10.1103/PhysRevLett.83.3940

[10] Barnabe, A., Maignan, A., Hervieu, M., Damay, F., Martin, C. and Raveau, B. (1997) Extension of Colossal Magnetoresistance Properties to Small a Site Cations by Chromium Doping in $Ln_{0.5}Ca_{0.5}MnO_3$ Manganites. *Applied Physics Letters*, **71**, 3907-3909. https://doi.org/10.1063/1.120540

[11] Kimura, T., Kumai, R., Okimoto, Y., Tomioka, Y. and Tokura, Y. (2000) Variation of Charge-Orbital Correlation with Cr Doping in Manganites. *Physical Review B*, **62**, 15021-15025. https://doi.org/10.1103/PhysRevB.62.15021

[12] Sun, Y., Tong, W., Xu, X.J. and Zhang, Y.H. (2001) Tuning Colossal Magnetoresistance Response by Cr Substitution in $La_{0.67}Sr_{0.33}MnO_3$. *Applied Physics Letters*, **78**, 643-645. https://doi.org/10.1063/1.1344229

[13] Lalitha, G., Das, D., Bahadur, D. and Venugopal Reddy, P. (2008) Elastic Behavior of $La_{0.67}Ca_{0.33}MnO_3$:ZrO_2 Composites. *Journal of Alloys and Compounds*, **464**, 6-8. https://doi.org/10.1016/j.jallcom.2007.09.097

[14] Buch, J.J.U., Lalitha, G., Pathak, T.K., Vasoya, N.H., Lakhani, V.K., Reddy, P.V., Kumar, R. and Modi, K.B. (2008) Structural and Elastic Properties of Ca-Substituted $LaMnO_3$ at 300K. *Journal of Physics D: Applied Physics*, **41**, Article ID: 025406. https://doi.org/10.1088/0022-3727/41/2/025406

[15] Wollan, E.O. and Koehler, W.C. (1955) Neutron Diffraction Study of the Magnetic Properties of the Series of Perovskite-Type Compounds $[(1-x)La, xCa]MnO_3$. *Physical Review Journals Archive*, **100**, 545-563. https://doi.org/10.1103/PhysRev.100.545

[16] Lalitha, G. and Venugopal Reddy, P. (2008) Elastic Behavior of Some Manganite-Based Orthorhombic $RMnO_3$ (R = Sm, Eu, Gd, Dy) Multiferroics. *Journal of Magnetism and Magnetic Materials*, **320**, 152-157. https://doi.org/10.1016/j.jmmm.2007.08.014

[17] Young, R.A. (1993) Introduction to the Rietveld Method. In: Young, R.A., Ed., *The*

Rietveld Method, Oxford University Press, Oxford, 1-38.

[18] Lalitha, G., Pavan Kumar, N. and Venugopal Reddy, P. (2018) Influence of Chromium Doping on Electrical and Magnetic Behavior of $Nd_{0.5}Sr_{0.5}MnO_3$ System. *Journal of Low Temperature Physics*, **192**, 133-144.
https://doi.org/10.1007/s10909-018-1922-3

[19] Lu, C.L., Ni, H., Yang, M., Xia, S.C., Wang, H.W., Wang, J.F. and Xia, Z.C. (2014) High Magnetic Field Phase Diagram in Electron-Doped Manganites La(0.4)Ca(0.6)Mn(1−y)Cr(y)O$_3$. *Scientific Reports*, **4**, Article No. 4902.
https://doi.org/10.1038/srep04902

[20] Lalitha, G. and Venugopal Reddy, P. (2009) Ultrasonic Velocity Studies in the Vicinity of T_C of Bismuth Doped Manganites. *Journal of Physics: Condensed Matter*, **21**, Article ID: 056003. https://doi.org/10.1088/0953-8984/21/5/056003

[21] Lalitha, G. and Venugopal Reddy, P. (2009) Elastic Behaviour of Strontium-Doped Lanthanum Calcium Manganites in the Vicinity of T_C. *Journal of Physics and Chemistry of Solids*, **70**, 960-966. https://doi.org/10.1016/j.jpcs.2009.05.005

[22] Anderson, O.L. (1965) 2-Determination and Some Uses of Isotropic Elastic Constants of Polycrystalline Aggregates Using Single-Crystal Data. In: Mason, W.P., Ed., *Physical Acoustics*, Vol. IIIB, Academic Press, New York, 43.
https://doi.org/10.1016/B978-0-12-395669-9.50009-6

[23] Wooster, W.A. (1953) Physical Properties and Atomic Arrangements in Crystals. *Reports on Progress in Physics*, **16**, 62-82.
https://doi.org/10.1088/0034-4885/16/1/302